PNAS RESEARCH ARTICLE | NEUROSCIENCE

Inositol hexakisphosphate kinase-2 non-catalytically regulates mitophagy by attenuating PINK1 signaling

Latika Nagpal[a,1], Michael D. Kornberg[b], and Solomon H. Snyder[a,c,d,1]

Contributed by Solomon H. Snyder; received December 3, 2021; accepted February 8, 2022; reviewed by Andrew Pieper and Dennis Stuehr

Inositol pyrophosphates, such as 5-diphosphoinositol pentakisphosphate (IP_7), are generated by a family of inositol hexakisphosphate kinases (IP6Ks), of which IP6K2 has been implicated in various cellular functions including neuroprotection. Absence of IP6K2 causes impairment of oxidative phosphorylation regulated by creatine kinase-B. In the present study, we show that IP6K2 is involved in attenuation of PINK1-mediated mitochondrial autophagy (mitophagy) in the brain. Up-regulation of dynamin-related protein (Drp-1), as well as increased expression of mitochondrial biogenesis markers (PGC1-α and NRF-1) in the cerebella of IP6K2-deleted mice (IP6K2-knockout), point to the involvement of IP6K2 in the regulation of mitochondrial fission. Knockdown of IP6K2 also leads to augmented glycolysis, potentially as a compensatory mechanism for decreased mitochondrial respiration. Overexpressing IP6K2 as well as IP6K2-kinase dead mutant in IP6K2-knockdown N2A cells reverses the expression of mitophagy markers, demonstrating that IP6K2-induced mitoprotection is catalytically/kinase independent. IP6K2 supplementation in K2-PINK1 double-knockdown N2A cells fails to reverse the expression of the mitophagic marker, LC3-II, indicating that the mitoprotective effect of IP6K2 is dependent on PINK1. Overall, our study reveals a key neuroprotective role of IP6K2 in the prevention of PINK1-mediated mitophagy in the brain.

inositol phosphate | mitophagy | PINK1 | neuroprotection | mitochondrial biogenesis

Significance

Inositol pyrophosphates are versatile messenger molecules containing the energetic pyrophosphate bond. One of the principal enzymes generating the inositol pyrophosphate IP_7 (5-diphosphoinositolpentakisphosphate) is inositol hexakisphosphate kinase 2 (IP6K2). Previous work has shown that IP6K2 is neuroprotective and maintains mitochondrial respiration. We now report that loss of IP6K2 leads to increased mitochondrial fission and mitophagy. Regulation of mitochondrial dynamics by IP6K2 depends on the protein PINK1 and, interestingly, is independent of IP6K2 enzymatic activity. These findings provide mechanistic insight into the regulation of mitochondrial function by IP6K2, which has implications for neuroprotection and mitochondrial physiology more generally.

Inositol pyrophosphates mediate various cellular and physiological functions, including regulation of insulin secretion, ATP production, DNA repair, Akt signaling, cell growth, apoptosis, and cell differentiation (1–5). Diphosphoinositol pentakisphosphate (IP_7) is the most extensively studied inositol pyrophosphate and displays a 5′-diphosphate (6, 7). IP_7 is generated in mammals by a family of inositol hexakisphosphate kinases (IP6Ks) that exist in three isoforms: IP6K1, IP6K2, and IP6K3 (8, 9).

Functions of the different forms of IP6K vary. IP6K2 was first reported as proapoptotic and has been implicated in cell death and apoptosis (10). Mice with deleted IP6K2 are resistant to ionizing radiation and display enhanced tumor formation. Cell survival mediated by heat-shock protein 90 (hsp-90) involves its binding to IP6K2 for catalytic inhibition of IP6K2, explaining why mutations blocking this binding activate IP6K2 to elicit cell death (11). Such cell death associated with activated IP6K2 is predominately mediated by p53 binding to IP6K2, resulting in decreased expression of proarrest gene targets, such as the cyclin-dependent kinase inhibitor, p21 (12). Similarly, casein kinase 2, which is up-regulated during tumor formation, elicits cell survival by phosphorylating and degrading IP6K2 (13). IP6K2 also regulates Purkinje cell morphology and motor coordination via protein 4.1N. Both IP6K2 and 4.1N are highly expressed in cerebellar granule cells (14). Besides the role of IP6K2 in cell death, inositol phosphates have also been associated with neuroprotection (15). Earlier, we showed that IP6K2 interacts with creatine kinase-B (CK-B) and regulates energy homeostasis (16). IP6K2 loss leads to decreased CK-B expression and reduced ATP levels, as well as diminished mitochondrial oxygen consumption rate associated with increased oxidative stress and decreased expression of cytochrome c1 of the complex III constituting the electron transport chain (16).

In the present study, we further assessed the role of IP6K2 in regulating cellular energy dynamics and mitochondrial functions in the cerebellum. We compared the mitochondrial morphology and biogenesis in IP6K2-knockout (KO) mice of different age groups (6, 12, and 24 mo). We report that the absence of IP6K2 leads to an enhanced expression of mitochondrial fission (dynamin-related protein-1, [Drp-1]) and biogenesis regulator proteins (peroxisome proliferator-activated receptor-γ coactivator 1-α [PGC1-α], nuclear respiratory factor-1 [NRF-1]), as well as mitophagy markers (PINK1, Parkin, and LC3-II) compared to the WT. We deployed a real-time Seahorse bioanalyzer to monitor extracellular acidification rate (ECAR) and proton efflux rate (PER) in WT and IP6K2-knockdown (KD) N2A cells and found that basal and

Author contributions: L.N. and S.H.S. designed research; L.N. and M.D.K. performed research; L.N., M.D.K., and S.H.S. analyzed data; and L.N. and S.H.S. wrote the paper.

Reviewers: A.P., Case Western Reserve University; and D.S., Cleveland Clinic Lerner College of Medicine of Case Western Reserve University.

The authors declare no competing interest.

[1]To whom correspondence may be addressed. Email: lnagpal1@jhmi.edu or ssnyder@jhmi.edu.

This article contains supporting information online at http://www.pnas.org/lookup/suppl/doi:10.1073/pnas.2121946119/-/DCSupplemental.

Published March 30, 2022.

compensatory glycolysis are augmented in K2-KD cells. Enhanced mitophagy in K2-KD cells was reversed by overexpressing IP6K2 in such cells. The reversal effects of mitophagy were similar in both IP6K2 and IP6K2-kinase dead-transfected N2A cells, indicating that the regulation of mitochondrial biogenesis and mitophagy by IP6K2 is catalytically kinase independent. We also observed no reversal in mitophagy by overexpressing IP6K2 in K2-PINK1 double-KD N2A cells indicating the specific mitoprotective role of IP6K2 in PINK1 mediated mitophagy. Our findings indicate that IP6K2 is a key regulator of mitochondrial homeostasis and promotes neuroprotection.

Results and Discussion

IP6K2 Deletion Promotes Mitochondrial Fission. In our previous study, we showed that IP6K2–CK-B interaction regulates energy homeostasis and mitochondrial functions associated with neuroprotection in the cerebellum (16). To assess the role of IP6K2 in regulating mitochondrial biogenesis, we examined mitochondrial morphology in the cerebella of different age groups (6, 12, and 24 mo) of WT and IP6K2-KO mice by transmission electron microscopy (TEM).

The overall mitochondrial morphology in a cell is dynamic and is controlled by a balance between mitochondrial fission and fusion. When both these events are balanced, the overall mitochondrial morphology remains relatively constant. However, if this balance is disrupted by a relative increase or decrease in either of the two processes due to any metabolic stress, the overall mitochondrial morphology can change drastically. In fusion-deficient cells, fission can lead to dissociation of mitochondria, with an increase in smaller independent organelles. Conversely, in fission-deficient cells, a relative increase in fusion elicits an interconnected network of mitochondrial tubules (17, 18)

In the present study, TEM analysis of WT and K2-KO cerebellar tissue sections revealed enhanced mitochondrial fission in K2-KOs compared to their WT counterparts, manifested as increased mitochondrial number and decreased mitochondrial size in the KO. However, the mitochondrial number decreased with age in both WT and K2-KO cerebellar sections (Fig. 1 *A* and *B*). Mitochondrial number was approximately two-fold higher in K2-KOs compared to WT at 6 mo of age (Fig. 1*B*). The mitochondrial number was significantly higher at a later age of 24 mo (approximately three-fold) in IP6K2-KOs (Fig.1*C*). Mitochondria were smaller both in size and area in KOs compared to the WTs (Fig. 1*D*). However, the overall ultrastructure of mitochondria was relatively normal in KOs. These results indicated higher mitochondrial fission in IP6K2-KO cerebellum, thereby establishing a role for IP6K2 in the maintenance of mitochondrial morphology.

IP6K2 Deletion Leads to Enhanced Expression of Mitochondrial Fission and Biogenesis Regulators, Drp-1, NRF-1, and PGC1-α and Decreased Expression of the Mitochondrial Fusion Protein, Mfn-1. Frequent fusion and fission facilitate the exchange of proteins and metabolites for maintenance of mitochondrial integrity. Imbalance in this dynamic process impairs mitochondrial function and has been implicated in diseases such as cancer, diabetes, and several neurodegenerative disorders (19–22). Mitochondrial fission is known to be up-regulated due to Drp1 activation in several types of tumors (23, 24). To determine whether IP6K2 also controls Drp-1 regulation, we performed immunoblotting of WT and IP6K2-KO cerebellar tissue lysates of different age groups (6, 12, and 24 mo) against Drp-1 and mitochondrial fusion (mitofusin-1, Mfn-1) protein regulators (Fig. 2*A*). Western blot analysis of Drp-1 indicated an ∼3-fold elevation in IP6K2-KO cerebellar tissue lysates in comparison to the WT (in 6-mo-old mice) and ∼2.3-fold elevation in IP6K2-KO mice in comparison to WT mice (in 12- and 24-mo old mice) (Fig. 2*A* and *SI Appendix*, Fig. S1 *A, A1*). In contrast, the mitochondrial fusion protein, Mfn-1, was down-regulated ∼50% (Fig. 2*A* and *SI Appendix*, Fig. S1 *A, A2*). The increase in mitochondrial number prompted us to examine mitochondrial biogenesis in IP6K2-KO mice. The key protein regulators of mitochondrial biogenesis PGC1-α and its downstream target NRF-1 were up-regulated by ∼2.1-fold and ∼3.2-fold, respectively, in IP6K2-KO mice cerebella compared to their WT counterparts (6-mo old mice) (Fig. 2*A* and *SI Appendix*, Fig. S1 *A, A3* and *A4*).

We also confirmed the protein expression changes of Drp-1, Mfn-1, PGC1-α, and NRF-1 in WT and K2-KD N2A and PC-12 cells. The corresponding Western blots are shown in Fig. 2*B* and the quantitation of the protein expression change is shown in *SI Appendix*, Fig. S1*B*. The level of depletion of IP6K2 using short-hairpin RNA (shRNA) in K2-KD N2A and PC-12 cells are quantified in *SI Appendix*, Fig. S1*C*. Immunofluorescence staining of IP6K2- KD N2A cells revealed a stronger staining for Drp-1 in KD cells compared to the WT cells (Fig. 2*C*). Overall, these results suggest that in absence of IP6K2, cells adopt selective mitochondrial dynamics that favor mitochondrial fission over fusion through up-regulation of Drp1 and the mitochondrial biogenesis regulators PGC1-α and NRF-1 and down-regulation of Mfn1.

Loss of IP6K2 Leads to Increased Glycolytic Capacity. We previously reported that loss of IP6K2 in the mouse cerebellum led to mitochondrial dysfunction and decreased ATP production along with an increase in reactive oxygen species (ROS) and oxidative stress (16). Increased mitochondrial ROS production is generally observed in pathological conditions characterized by mitochondrial dysfunction. Increase in ROS is also observed in multiple types of cancer (e.g., breast, pancreatic, ovarian, prostate, liver), neurodegenerative diseases (e.g., Alzheimer's disease and Parkinson's disease), as well as in type I and type II diabetes (25–28). Many of these diseases display enhanced glycolytic activity and impaired oxidative phosphorylation.

To understand the association between ROS, glucose metabolism, and IP6K2 expression, we examined glycolytic function in WT and IP6K2-KD N2A cells using two distinct Seahorse extracellular flux assays: a glycolytic stress test assay, which uses the ECAR as a proxy measure of lactate production, and the glycolytic rate assay, which uses PER as the measure of lactate. A schematic for the glycolysis stress test assay is depicted in Fig. 3*A*, in which basal glycolysis is measured as the increase in ECAR after addition of glucose and glycolytic capacity is the further increase in ECAR after inhibition of mitochondrial respiration with oligomycin. The glycolytic rate assay, in contrast, is performed in the presence of glucose from onset, with basal glycolysis measured as PER prior to inhibition of respiration with rotenone and antimycin A. IP6K2-KD cells exhibited a higher rate of basal glycolysis, as well as increased maximal glycolytic capacity compared to WT cells, as assessed by both assays (Fig. 3 *B* and *C*).

Quantitative analysis showed an increase in the basal glycolysis and glycolytic capacity by ∼4.5 and ∼4-fold, respectively, in K2-KD N2A cells compared to the WT cells (Fig. 3*D*) using ECAR, and an increase in compensatory glycolysis by ∼3-fold by measuring PER (Fig. 3*E*). These findings reveal an interplay

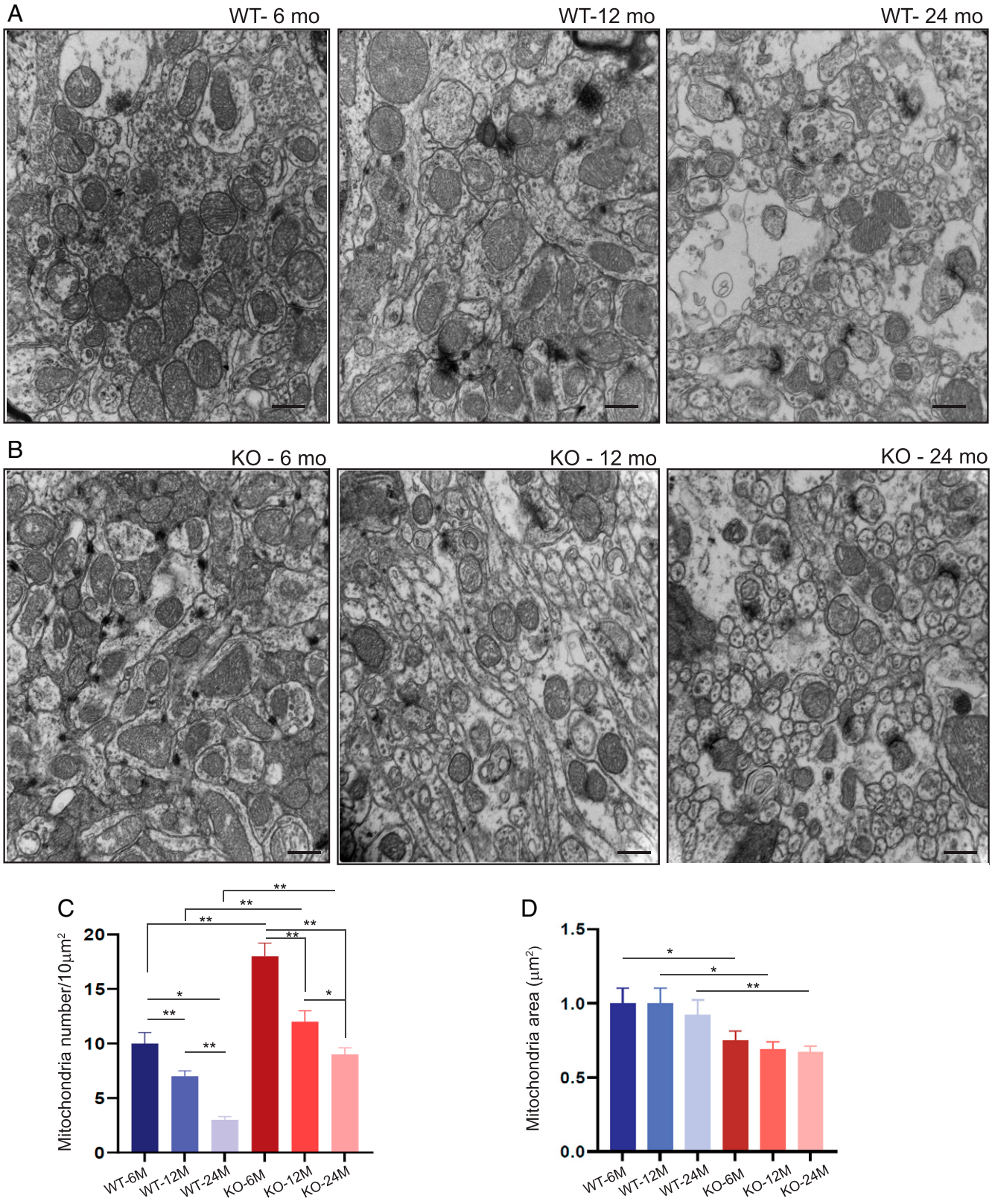

Fig. 1. IP6K2 deletion leads to increase in mitochondrial fission. Electron microscopic analysis of the cerebellar molecular layer from IP6K2-KO (6, 12 and 24 mo) revealed higher mitochondrial fission compared to the respective WT sections (*A* and *B*). However, the ultrastructure of mitochondria in the IP6K2-KO cerebella was relatively normal. (Scale bars, 500 nm.) (*C*) Number of mitochondria were two-fold higher in K2-KO cerebellar tissue sections compared to their WT counterparts at 6 and12 mo age and approximately three-fold higher at 24 mo, whereas the mitochondria were smaller both in size and area in KO compared to the WT (*D*). Significant differences are $^{**}P < 0.01$, $^{*}P < 0.05$, analyzed by one-way and two-way ANOVA. Data represent mean ± SD of $n = 6$ per age group and 5 different cerebellar sections analyzed per animal. Further details of the experiment are described in *Materials and Methods*.

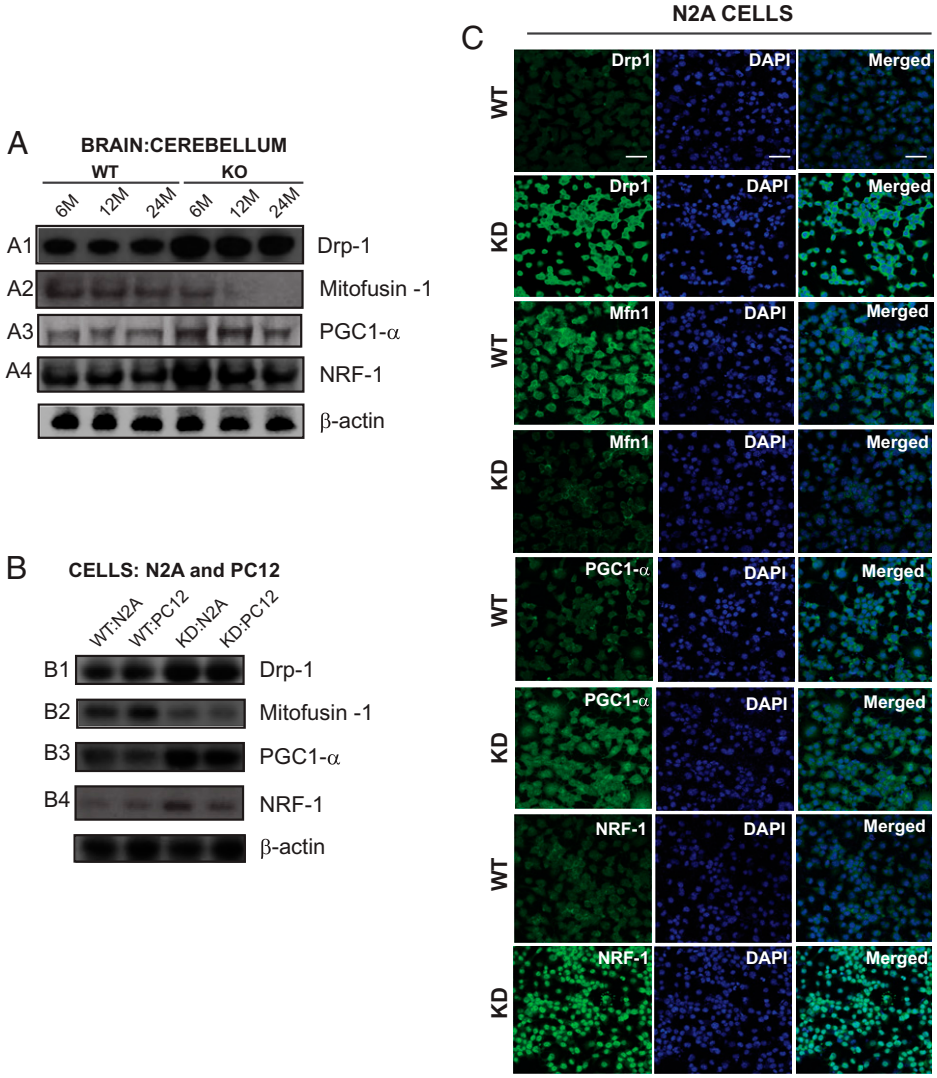

Fig. 2. IP6K2 deletion elicits up-regulation of mitochondrial fission and biogenesis regulators. (*A*) Western blot analyses of mitochondrial biogenesis regulators (Drp1, Mfn1, PGC1-α, and NRF-1) were performed in cerebellar lysates of WT and IP6K2-KO mice of ages 6, 12, and 24 mo. N2A and PC-12 cells were transfected with IP6K2 shRNA (for eliciting IP6K2-KD) and protein expression of Drp-1, Mfn-1, PGC1-α, and NRF-1 were assessed in WT and IP6K2- KD cells using immunoblotting (*B*), as well as immunofluorescence imaging using a confocal microscope Quantitation of the protein blots in *A* and *B* are shown in *SI Appendix*, Fig. S1. (*C*) Alexa-488 secondary antibody (green) was used for immunostaining the depicted mitochondrial fission, fusion, and biogenesis markers respectively(Drp-1, Mfn-1, PGC1-α and NRF-1). (Scale bar, 20 μm.)

between IP6K2, ROS, and glucose metabolism with increased glycolysis possibly as a compensatory response to impaired mitochondrial respiration as observed in our previous study (16). In other cell types, such as dendritic cells, glycolytic up-regulation has been demonstrated as a necessary compensatory response to decreased mitochondrial respiration (29)

High glucose levels induce mitochondrial fragmentation in cells, which is a prerequisite for increased ROS production. However, mitochondrial fission induced by overexpression of the fission-promoting protein, Drp1, does not stimulate ROS levels (30, 31).

Based on our findings, we speculate that fragmented mitochondria produced in IP6K2-KO cerebella produce more ROS, probably due to a relatively higher surface area that allows better uptake of metabolic substrates as compared to WTs. In addition, due to higher glycolytic capacity in IP6K2-KD N2A cells, there is an increased glycolytic conversion to pyruvate. An impaired complex III of the electron transport chain also leads to an increase in oxidative stress in N2A cells deficient in IP6K2 (16), suggesting that increased ROS levels may not be causally associated with the observed mitochondrial fission in our study.

Loss of IP6K2 Leads to Kinase-Independent Mitophagy that Is Reversed by Restoring IP6K2 Levels in Cells. The autophagic elimination of mitochondria or mitophagy is closely linked to mitochondrial fission. Mitophagy can be prevented by a dominant-negative mutant of Drp1, suggesting that fission is required for mobilizing such cellular degeneration (32). Damaged mitochondria undergo selective mitophagy (33), which is also consistent with the fission event as it elicits quality control by segregating the damaged mitochondria and eliminating them through autophagy. Mitophagy is usually regulated by one of the following three pathways: FUNDC1, BNIP3/NIP3-Nix pathway (hypoxia-induced), or PINK1/Parkin mediated pathway (non-hypoxia induced) (34). To examine the precise role of mitophagy regulators, we determined the protein expressions of prominent mitophagy markers of these three pathways controlling mitochondrial health: BNIP3, BNIP3-Nix, PINK1, NDP52, SQSTM1/p62, Parkin, and optineurin in WT, and K2-KD N2A cell lysates. We found no significant change in protein expression in BNIP3, BNIP3/Nix, NDP52, and optineurin. However, there was an increase of ∼2-fold in SQSTM1/p62 and ∼2.5-fold in PINK1, Parkin expression in K2-KD N2A cells compared to the WT cells (Fig. 4 *A* and *B*).

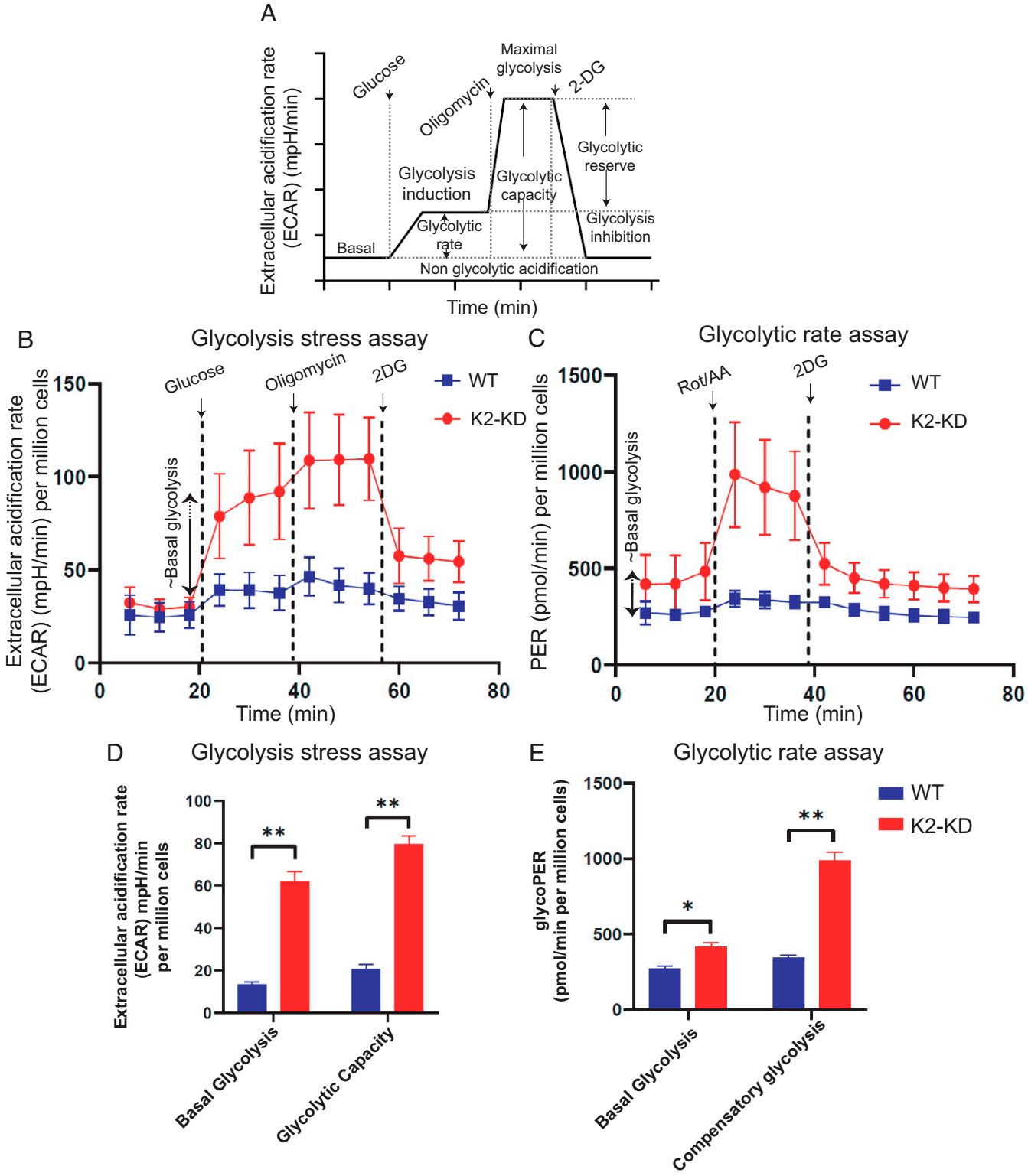

Fig. 3. Functional characterization of glycolysis in IP6K2-KD N2Acells. (*A*) Schematic representation of real-time glycolysis. ECAR analysis starts from basal ECAR, in which the cells are incubated in glucose-free media followed by the addition of glucose (for induction of glycolysis), oligomycin (for induction of maximal cell glycolysis and complex V inhibition), and 2-DG (for inhibition of glycolysis). Glycolytic rate (glycolysis induction subtracted for basal ECAR) is derived from the ECAR curve. (*B*) Glycolytic function was measured as ECAR using a Seahorse extracellular flux analyzer in WT and K2-KD cells. (*C*) Glycolytic rate was measured in WT and K2-KD cells to determine the glycoPER. (*D*) Quantitative estimation of glycolytic function and (*E*) glycolytic rate was measured as basal ECAR levels, glycolytic capacity, basal glycoPER, and compensatory glycolysis. Data are based on multiple *t*-tests analysis with false-discovery rate testing and are representative of a minimum of 8 replicates per group. $^{**}P < 0.01$, $^{*}P < 0.05$.

Under nonhypoxic conditions, the mitochondrial quality control is governed majorly by two protein factors: PINK1 and Parkin. PINK1 is constitutively repressed in healthy mitochondria through import into the inner mitochondrial membrane and degradation by the protease PARL. When mitochondria become uncoupled, protein import to the inner mitochondrial membrane is prevented so PINK1 is diverted from PARL and accumulates on the outer mitochondrial membrane. This acts as

a sensor for mitochondrial damage that distinguishes impaired mitochondria from healthy ones. PINK1 recruits the E3-ligase Parkin specifically on impaired mitochondria. Parkin then ubiquitinates outermitochondrial membrane proteins and induces autophagic elimination of the flagged mitochondrion (35).

To assess the precise role of mitophagy in the observed mitochondrial changes triggered by the absence of IP6K2 in the cerebella of mice of different age groups, we analyzed the expression levels of the mitophagy markers PINK1, Parkin, and LC3-II in the cerebella of 6-, 12-, and 24-mo-old mice. Levels of PINK1, Parkin, and LC3-II were significantly elevated in the cerebellar tissue lysates from IP6K2-KO mice. Protein expression of PINK1 and Parkin was respectively elevated ∼2-fold and ∼2.5-fold in 6-mo-old KO mice. However, the expression of Parkin but not PINK1 proteins was reduced with age in 6-, 12-, and 24-mo mice in KOs compared to their respective WTs. LC3-II was up-regulated to ∼1.5-fold and 1.8-fold in IP6K2-KO cerebella in 12- and 24-mo-old mice, respectively, compared to their WT counterparts (Fig. 4*C*). Data are quantified and represented in the graphs depicted in *SI Appendix*, Fig. S2. Autophagic vacuoles seen during mitophagy were also observed in the cerebellar tissue section of K2-KOs of 24-mo-old mice. The TEM images are shown in *SI Appendix*, Fig. S3.

To further analyze whether the kinase activity of IP6K2 is involved in regulating mitophagy, we transfected IP6K2 and IP6K2 kinase dead mutant (K222A) into N2A cells. Cell lysates were subsequently blotted with antibodies against the mitophagy markers PINK1, Parkin, and LC3-II (Fig. 4*D*). We observed an ∼35% reversal in PINK1 expression, ∼55% reversal in Parkin, and ∼35% reversal in LC3-II expression in cells transfected with K2 (K2-R) and K222A K2 (K222A-R) (kinase dead) (Fig. 4*E*). These observations imply that regulation of mitophagy by IP6K2 does not depend on its kinase activity.

As we observed changes in protein expression for PINK1, Parkin, and SQSTM/p62 in N2A cells lacking IP6K2 (Fig. 4 *A* and *B*), we used K2-PINK1 and K2-SQSTM1/p62 double-KD cells to further understand whether K2 directly regulates mitophagy through PINK1/Parkin or SQSTM1/p62 (Fig. 4*F*). We transfected K2-PINK1 and K2-SQSTM1/p62 double-KD cells with full-length IP6K2. We observed a decrease in LC3-II expression in SQSTM1/p62-KD cells on overexpressing K2 but not in the cells in which PINK1 was knocked down. This indicates that K2-mediated mitoprotection is regulated through PINK1, leading us to suggest that IP6K2 directly controls the PINK1/Parkin mitophagy pathway. We also observed an increase (∼27%) in the glycolytic assay in PINK1-KD cells as compared to WT (*SI Appendix*, Fig. S4). Overall, our observations indicate that IP6K2 plays a critical neuroprotective role by regulating mitophagy and mitochondrial morphology by suppressing PINK1 expression. Deciphering the precise mechanism by which IP6K2 influences the expression of PINK1 while manifesting its mitoprotective role would admittedly require further investigation.

In summary, our study reveals that cells and animals lacking IP6K2 adopt an upregulation of mitophagy and mitochondrial biogenesis during the selective dynamics favoring mitochondrial fission (Figs. 1 and 2). Moreover, with upregulation of mitochondrial fission, augmented mitophagy and glycolytic capacity was observed in IP6K2-deleted cells and animals (Figs. 3 and 4).

Fission segregates damaged mitochondria to preserve the health of the mitochondrial network, in addition to regulating morphology and facilitating mitochondrial trafficking and mitophagy. The dynamic mitochondrial fusion and fission cycle balances two competing processes: compensation for damage by fusion and elimination of damage by fission. Failure of these stress responses may lead to neuronal death and neurodegenerative disorders. It is noteworthy that the mitochondrial fission pathway via Drp-1 is regulated by IP6K2. Because a basal mitochondrial function is required for cells with higher glycolysis, as well as increased ROS and oxidative stress, up-regulation of PGC1-α and NRF-1–mediated mitochondrial biogenesis may play critical roles in meeting such a requirement, particularly in the case of augmented mitochondrial turnover (mitophagy) regulated by Drp-1 and IP6K2. Thus, our study indicates that IP6K2 regulates mitoprotection by suppressing PINK1 expression and attenuating the PINK1/Parkin-mediated mitophagy pathway.

These findings highlight the importance of considering both mitochondrial biogenesis and mitophagy for the effective treatment of neurodegenerative diseases mediated by mitochondrial dysfunction and enhanced oxidative stress. Thus, in-depth understanding of the underlying mitophagic processes may facilitate the development of more effective treatments for mitochondrial and neurodegenerative diseases.

Materials and Methods

Reagents. Anti-IP6K2 antibody was purchased from Sigma-Aldrich. Antibodies against Drp-1, PGC1-α, NRF-1, PINK1, Parkin, SQSTM1, LC3-II, and mitophagy markers kit were procured from Cell Signaling Technologies. Alexa Fluor-488 goat anti-rabbit and anti-mouse antibodies were purchased from Life Technologies. IP6K2 shRNA, PINK1 shRNA, SQSTM1/p62 shRNA, and control shRNA plasmids were procured from Santa Cruz Biotechnology.

Animals. Both male and female C57BL/6 WT and IP6K2-KO mice of 6, 12, and 24 mo of age were used for animal-based experiments. Animal breeding and procedures were conducted in strict accordance with the NIH *Guide for the Care and Use of Laboratory Animals* (36). Animal experiments were approved by the Johns Hopkins University Animal Care and Use Committee. Animals were kept on a 12-h light/dark cycle and were provided food and water ad libitum.

Transmission Electron Microscopy. Mice were perfused with 2% glutaraldehyde and 2% paraformaldehyde in 0.1 M sodium cacodylate buffer with 3 mM magnesium chloride, followed by dissection, and buffer rinses in 0.1 M sodium cacodylate. Secondary fixation was done with 2% osmium in 0.1 M sodium cacodylate reduced with 1.6% potassium ferrocyanide for 2 h at 4 °C, followed by water rinses, *en bloc* staining with 2% uranyl acetate (aq.), and then dehydration with a graded series of ethanol before embedding in EPON resin. Regions of interest were identified with semi-thin (0.3 μm) sections stained with Toluidine blue, and the ultrathin sections (70 to 90 nm) were collected on formvar coated 2 × 1-mm copper slot grids and stained with uranyl acetate (2%) and lead citrate (0.3%). Samples were imaged on a Hitachi 7600 TEM at 80 kV with an AMT XR80 CCD (8 megapixel, 16-bit camera). Mitochondria were counted from at least six different fields of view.

Cell Culture and Transfection Conditions. N2A neuronal cells were grown in a humid atmosphere of 5% CO_2 at 37 °C in DMEM supplemented with 10% FBS, L-glutamine (2 mM), penicillin (100 U/mL), and streptomycin (100 μg/mL). Cells were transfected using Lipofectamine LTX and incubated for 10 to 12 h before the transfection medium was replaced with a serum-containing medium. Cells were transfected with full-length IP6K2 as well as a mutant form of IP6K2 wherein lysine-222 is transformed to alanine (K222A). K222A lacks catalytic kinase activity (9).

Immunofluorescence Staining and Confocal Microscopy. For immunofluorescence staining of N2A cells, cells were grown in chamber slides, fixed using 4% paraformaldehyde, and permeabilized by incubation with 0.01% Triton X-100 at 4 °C for 5 min (37). Nonspecific sites were then blocked by incubation with 5% goat serum. Subsequently, the cells were incubated with the primary antibodies (1:100) overnight in a humid chamber following which the cells were

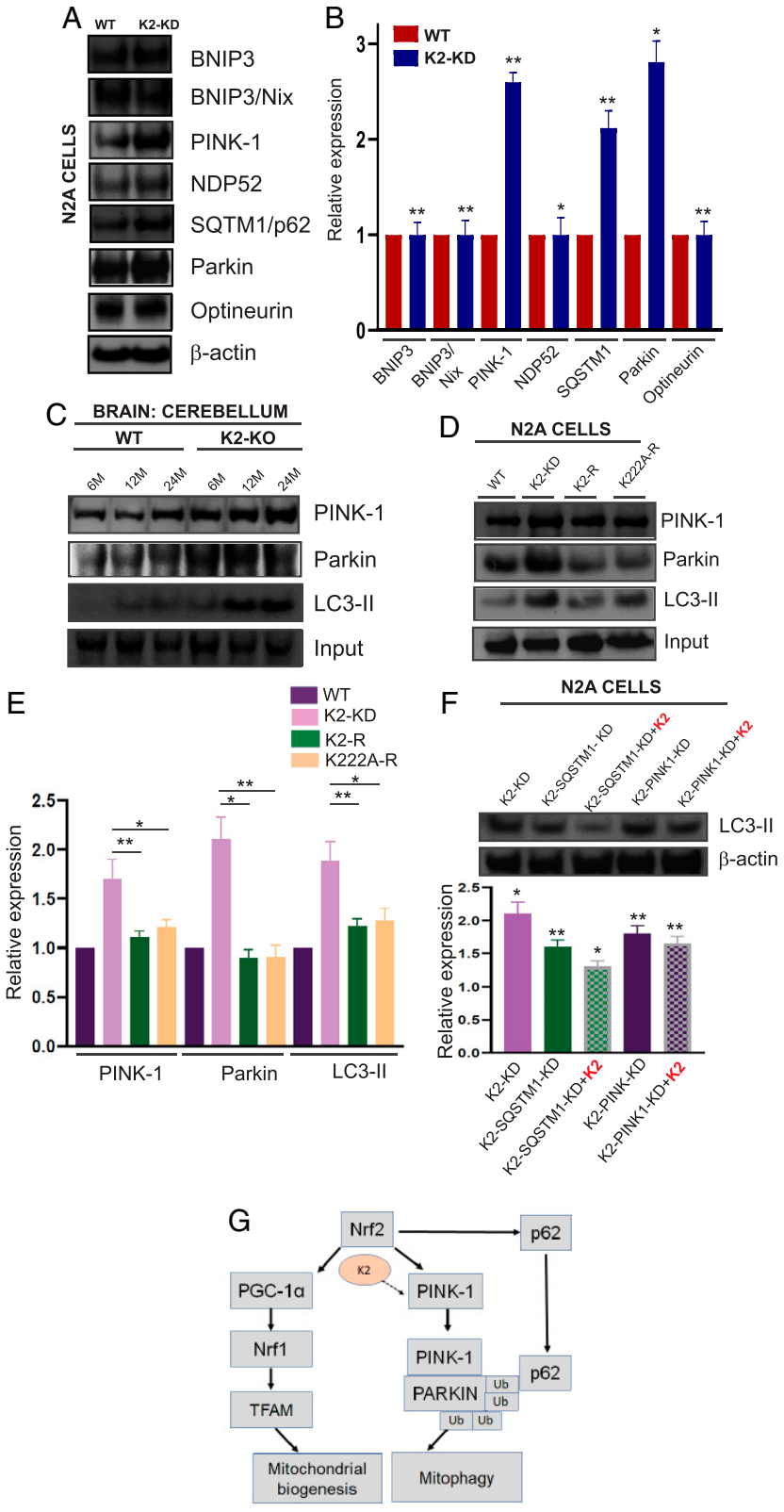

Fig. 4. IP6K2 induced mitoprotection is kinase independent and suppresses PINK1-mediated mitophagy pathway. (*A*) Protein expressions of different mitophagic factors (BNIP3, BNIP3/Nix, PINK1, NDP52, SQSTM1/p62, Parkin, and optineurin) were determined through Western blot analyses of cell lysates of WT and K2-KD N2A cells. (*B*) Quantitative analysis of the protein expressions in *A*. (*C*) Analysis of mitophagy regulators in cerebellar lysates of WT and K2-KO mice of 6, 12, and 24 mo through protein expression assessment of PINK1, Parkin, LC3-II using Western blotting. Data are quantified and represented in the graphs depicted in *SI Appendix*, Fig. S2. (*D*) Full-length IP6K2 (K2) and IP6K2 kinase dead mutant (K222A) were transfected into K2-KD N2A cells. Representative immunoblots of the lysates from WT, K2-KD, and N2A cells transfected with K2 (K2-R) and K222A cells (K222A-R) were blotted against PINK1, Parkin, LC3-II antibodies. Immunoblot protein bands are quantified in *E*. (*F*) Full-length K2 was transfected in K2-SQSTM1/p62 and K2-PINK1 double-KD cells. Cell lysates from K2-KD cells, K2-SQSTM1/p62 double-KD cells, K2-PINK1 double-KD cells, and K2 supplemented SQSTM1/p62 and PINK1 cells were immunoblotted against LC3-II. The corresponding Western blot, as well as the quantitative analysis of protein bands, are depicted in *F*. (*G*) Scheme of IP6K2-mediated mitophagy regulation. Data are presented as mean ± SD and are representative of three independent experiments performed under identical conditions. Significant differences are $^{**}P < 0.01$, $^{*}P < 0.05$, analyzed by one-way ANOVA. Further details of the experiment are described in *Materials and Methods*.

stained with respective fluorescent secondary antibodies (1:300). Nuclei were counterstained with DAPI. Images were captured and analyzed using a confocal microscope (LSM 700, Zeiss).

Immunoblotting. Cells and cerebellar tissues were lysed by sonication in lysis buffer supplemented with protease inhibitors. Protein concentrations were measured by Bradford assay (Bio-Rad). Lysates were mixed with SDS sample buffer, boiled, and resolved by SDS/PAGE. Bands were transferred to PVDF Immobilon membranes (Millipore) using a wet transfer. Membranes were blocked in TBS-T containing 1% BSA, and probed overnight at 4 °C with primary antibody and thereafter with HRP-conjugated secondary antibodies (GE Healthcare-Amersham) for 1 to 2 h. The immunoblots were washed and visualized using the ImmunoCruz luminol reagent (Santa Cruz Biotechnology) followed by film exposure. Quantification of digitally scanned immunoblots was performed by densitometry analysis using ImageJ software.

Seahorse Extracellular Flux Analyzer Assay for Glycolysis. WT and K2-KD N2A cells were harvested and seeded directly into Seahorse XF96 cell culture microplates. After overnight culture, the medium was removed, and cells were washed once with sterile PBS and fresh MEM-complete medium was added. After 18 to 24 h at 37 °C, the medium was changed to Seahorse XF assay medium (glucose-free for glycolysis stress test assay) containing 2 mM glutamine (pH adjusted to 7.4 and sterile-filtered), and cells were kept at 37 °C in a CO_2-free incubator for an additional 45 min to 1 h before the assay. The ECAR was measured using a Seahorse XFe96 Analyzer. Sensor cartridges were pre-hydrated in XF calibrant solution overnight in a CO_2-free incubator. For the glycolysis stress test assay, ports were loaded with glucose (Port A), oligomycin (Port B), and 2-deoxyglucose (2-DG) (Port C) to achieve concentrations of 10 mM, 1 μM, and 50 mM, respectively, after injection. Three measurements were obtained prior to each port injection, and after injection of Port C, with a measurement loop of 1-min mix, 2-min wait, and 3-min measure. Data were analyzed using the XF Glycolysis Stress Test Report Generator. For the glycolytic rate assay, the medium was supplemented with 5 mM glucose, 2 mM glutamine, 1 mM sodium pyruvate, pH 7.4. Then, ECAR and oxygen consumption rate were recorded using the Seahorse XF24e analyzer, following injections with 4 μM Rotenone/Antimycin A and 50 mM 2-DG, respectively. The PER, glycoPER, basal glycolysis, and compensatory glycolysis were calculated from this assay. All assay results were analyzed using the Wave program 2.3.0 (Agilent Technologies).

Image Quantification and Statistical Analysis. Images were quantified with ImageJ software. For Western blots, the expression changes of the proteins were evaluated by normalizing their recorded band intensities against their input band (β-actin). Data are presented as the mean ± SD from at least three independent experiments conducted under similar conditions. The *P* values were calculated by one-way or two-way ANOVA.

Data Availability. All study data are included in the main text and *SI Appendix*.

ACKNOWLEDGMENTS. We thank Prof. Ahmet Hoke for providing access to the Seahorse extracellular flux analyzer; Barbara Smith, Cell Biology Imaging Facility, The Johns Hopkins University School of Medicine, for helping us with sample preparation and analysis by electron microscopy; and Lauren Albacarys, Lynda Hester, Roxanne Barrow, Virginia Miller, and Susan McTeer for their excellent technical support. This work was supported by US Public Health Service Grant MH18501 and DA044123.

Author affiliations: [a]The Solomon H. Snyder Department of Neuroscience, The Johns Hopkins University School of Medicine, Baltimore, MD 21205; [b]Department of Neurology, The Johns Hopkins University School of Medicine, Baltimore, MD 21287; [c]Department of Psychiatry and Behavioral Sciences, The Johns Hopkins University School of Medicine, Baltimore, MD 21287; and [d]Department of Pharmacology and Molecular Sciences, The Johns Hopkins University School of Medicine, Baltimore, MD 21205

1. C. Illies *et al.*, Requirement of inositol pyrophosphates for full exocytotic capacity in pancreatic beta cells. *Science* **318**, 1299–1302 (2007).
2. Z. Szigyarto, A. Garedew, C. Azevedo, A. Saiardi, Influence of inositol pyrophosphates on cellular energy dynamics. *Science* **334**, 802–805 (2011).
3. A. Chakraborty *et al.*, Inositol pyrophosphates inhibit Akt signaling, thereby regulating insulin sensitivity and weight gain. *Cell* **143**, 897–910 (2010).
4. R. S. Jadav, M. V. Chanduri, S. Sengupta, R. Bhandari, Inositol pyrophosphate synthesis by inositol hexakisphosphate kinase 1 is required for homologous recombination repair. *J. Biol. Chem.* **288**, 3312–3321 (2013).
5. F. Rao *et al.*, Inositol pyrophosphates mediate the DNA-PK/ATM-p53 cell death pathway by regulating CK2 phosphorylation of Tti1/Tel2. *Mol. Cell* **54**, 119–132 (2014).
6. C. J. Barker, C. Illies, G. C. Gaboardi, P. O. Berggren, Inositol pyrophosphates: Structure, enzymology and function. *Cell. Mol. Life Sci.* **66**, 3851–3871 (2009).
7. S. B. Shears, Diphosphoinositol polyphosphates: Metabolic messengers? *Mol. Pharmacol.* **76**, 236–252 (2009).
8. A. Saiardi, H. Erdjument-Bromage, A. M. Snowman, P. Tempst, S. H. Snyder, Synthesis of diphosphoinositol pentakisphosphate by a newly identified family of higher inositol polyphosphate kinases. *Curr. Biol.* **9**, 1323–1326 (1999).
9. A. Saiardi, E. Nagata, H. R. Luo, A. M. Snowman, S. H. Snyder, Identification and characterization of a novel inositol hexakisphosphate kinase. *J. Biol. Chem.* **276**, 39179–39185 (2001).
10. B. H. Morrison, J. A. Bauer, D. V. Kalvakolanu, D. J. Lindner, Inositol hexakisphosphate kinase 2 mediates growth suppressive and apoptotic effects of interferon-beta in ovarian carcinoma cells. *J. Biol. Chem.* **276**, 24965–24970 (2001).
11. A. Chakraborty *et al.*, HSP90 regulates cell survival via inositol hexakisphosphate kinase-2. *Proc. Natl. Acad. Sci. U.S.A.* **105**, 1134–1139 (2008).
12. M. A. Koldobskiy *et al.*, p53-mediated apoptosis requires inositol hexakisphosphate kinase-2. *Proc. Natl. Acad. Sci. U.S.A.* **107**, 20947–20951 (2010).
13. A. Chakraborty *et al.*, Casein kinase-2 mediates cell survival through phosphorylation and degradation of inositol hexakisphosphate kinase-2. *Proc. Natl. Acad. Sci. U.S.A.* **108**, 2205–2209 (2011).
14. L. Nagpal, C. Fu, S. H. Snyder, Inositol hexakisphosphate kinase-2 in cerebellar granule cells regulates Purkinje cells and motor coordination via protein 4.1N. *J. Neurosci.* **38**, 7409–7419 (2018).
15. Z. Zhang *et al.*, Neuroprotection of inositol hexaphosphate and changes of mitochondrion mediated apoptotic pathway and α-synuclein aggregation in 6-OHDA induced parkinson's disease cell model. *Brain Res.* **1633**, 87–95 (2016).
16. L. Nagpal, M. D. Kornberg, L. K. Albacarys, S. H. Snyder, Inositol hexakisphosphate kinase-2 determines cellular energy dynamics by regulating creatine kinase-B. *Proc. Natl. Acad. Sci. U.S.A.* **118**, e2020695118 (2021).
17. D.-F. Suen, K. L. Norris, R. J. Youle, Mitochondrial dynamics and apoptosis. *Genes Dev.* **22**, 1577–1590 (2008).
18. H. Sesaki, R. E. Jensen, Division versus fusion: Dnm1p and Fzo1p antagonistically regulate mitochondrial shape. *J. Cell Biol.* **147**, 699–706 (1999).
19. T. Wai, T. Langer, Mitochondrial dynamics, and metabolic regulation. *Trends Endocrinol. Metab.* **27**, 105–117 (2016).
20. C. Osman, T. R. Noriega, V. Okreglak, J. C. Fung, P. Walter, Integrity of the yeast mitochondrial genome, but not its distribution and inheritance, relies on mitochondrial fission and fusion. *Proc. Natl. Acad. Sci. U.S.A.* **112**, E947–E956 (2015).
21. Z. Cheng *et al.*, Foxo1 integrates insulin signaling with mitochondrial function in the liver. *Nat. Med.* **15**, 1307–1311 (2009).
22. J. Zhao *et al.*, Mitochondrial dynamics regulates migration and invasion of breast cancer cells. *Oncogene* **32**, 4814–4824 (2013).
23. J. A. Kashatus *et al.*, Erk2 phosphorylation of Drp1 promotes mitochondrial fission and MAPK-driven tumor growth. *Mol. Cell* **57**, 537–551 (2015).
24. A. Ferreira-da-Silva *et al.*, Mitochondrial dynamics protein Drp1 is overexpressed in oncocytic thyroid tumors and regulates cancer cell migration. *PLoS One* **10**, e0122308 (2015).
25. J. D. Hayes, A. T. Dinkova-Kostova, K. D. Tew, Oxidative stress in cancer. *Cancer Cell* **38**, 167–197 (2020).
26. I. V. Turko *et al.*, Protein tyrosine nitration in the mitochondria from diabetic mouse heart. Implications to dysfunctional mitochondria in diabetes. *J. Biol. Chem.* **278**, 33972–33977 (2003).
27. F. Yin, H. Sancheti, I. Patil, E. Cadenas, Energy metabolism and inflammation in brain aging and Alzheimer's disease. *Free Radic. Biol. Med.* **100**, 108–122 (2016).
28. A. Anandhan *et al.*, Metabolic dysfunction in Parkinson's disease: Bioenergetics, redox homeostasis and central carbon metabolism. *Brain Res. Bull.* **133**, 12–30 (2017).
29. B. Everts *et al.*, Commitment to glycolysis sustains survival of NO-producing inflammatory dendritic cells. *Blood* **120**, 1422–1431 (2012).
30. T. Yu, B. S. Jhun, Y. Yoon, High-glucose stimulation increases reactive oxygen species production through the calcium and mitogen-activated protein kinase-mediated activation of mitochondrial fission. *Antioxid. Redox Signal.* **14**, 425–437 (2011).
31. F. Distelmaier *et al.*, Trolox-sensitive reactive oxygen species regulate mitochondrial morphology, oxidative phosphorylation and cytosolic calcium handling in healthy cells. *Antioxid. Redox Signal.* **17**, 1657–1669 (2012).
32. G. Twig *et al.*, Fission and selective fusion govern mitochondrial segregation and elimination by autophagy. *EMBO J.* **27**, 433–446 (2008).
33. I. Kim, J. J. Lemasters, Mitophagy selectively degrades individual damaged mitochondria after photoirradiation. *Antioxid. Redox Signal.* **14**, 1919–1928 (2011).
34. W.-X. Ding, X.-M. Yin, Mitophagy: Mechanisms, pathophysiological roles, and analysis. *Biol. Chem.* **393**, 547–564 (2012).
35. D. Narendra, A. Tanaka, D. F. Suen, R. J. Youle, Parkin is recruited selectively to impaired mitochondria and promotes their autophagy. *J. Cell Biol.* **183**, 795–803 (2008).
36. National Research Council, *Guide for the Care and Use of Laboratory Animals* (National Academies Press, Washington, DC, ed. 8, 2011).
37. L. Nagpal *et al.*, Mechanism of inducible nitric-oxide synthase dimerization inhibition by novel pyrimidine imidazoles. *J. Biol. Chem.* **288**, 19685–19697 (2013).